ELSEVIER

Journal of Crystal Growth 204 (1999) 213–223

JOURNAL OF CRYSTAL GROWTH

www.elsevier.nl/locate/jcrysgro

Analysis of the unsteady segregation in crystal growth from a melt I. Fluctuating interface velocity

F.Z. Haddad[a,*], J.P. Garandet[b], D. Henry[a], H. Ben Hadid[a]

[a]*Laboratoire de Mécanique des Fluides et d'Acoustique, Ecole Centrale de Lyon/UCB Lyon 1, UMR CNRS 5509, ECL, BP 163, 69131 Ecully Cedex, France*

[b]*Commissariat à l'Energie Atomique, DTA/CEREM/DEM/SPCM/LRBS, CEA Grenoble, 17 Rue des Martyrs, 38054 Grenoble Cedex 9, France*

Received 22 September 1998; accepted 5 February 1999
Communicated by D.T.J. Hurle

Abstract

The purpose of this paper is to analyse the correlations between interface velocity fluctuations and segregation in the crystal during solidification in the horizontal Bridgman configuration. The effects of both the amplitude and the frequency of the interface velocity oscillations on the axial and radial segregation will be determined. The results will be compared with predictions based on an analytical model.

Keywords: Segregation; Bridgman; Instationarity

1. Introduction

In alloy crystal growth of application oriented materials (e.g. substrate manufacture for the electronic industry), composition striations resulting from unsteady solidification conditions are known to be a serious problem [1]. Apparatus-related instabilities, such as rotation in an asymmetrical thermal field, vibrations or pulling rate variations, lead to fluctuations of the solidification velocity and in turn of the crystal composition, as clearly demonstrated experimentally [2]. Unsteady convection in the melt may act directly on the solute field, as in the case of *g*-jitters in microgravity solidification [3] but also indirectly via the induced variations of the growth rate if the coupling with heat transport is strong enough. Atomic-scale kinetic effects, such as step bunching on faceted interfaces [4,5], can also result in transient solute incorporation.

Even at the continuum level, an analytical solution to the problem of solute striations is a formidable task, since it requires the time-dependent versions of the heat, momentum and mass conservation equations to be solved simultaneously. In their pioneering work, Hurle et al. [6] focused on the effect of a thermal fluctuation on the composition field, and used the stagnant film model originally proposed by Burton et al. [7] to account for convective transport. This approach was later refined by Thevenard et al. [8] to lift some minor flaws in the formulation. More recently, the stagnant film

* Corresponding author.
E-mail address: haddad@mecaflu.ec-lyon.fr (F.Z. Haddad)

0022-0248/99/$ - see front matter
PII: S0022-0248(99)00093-7

Nomenclature

C	solute composition (mass fraction)
D	solute diffusion coefficient ($m^2\ s^{-1}$)
g	gravity ($m\ s^{-2}$)
H	typical dimension of the cavity (m)
k	solute partition coefficient of the binary alloy ($k = 0.087$)
V	mass average velocity of the Navier–Stokes equation ($m\ s^{-1}$)
V_{eff}	effective transport velocity ($m\ s^{-1}$)
V_I	interface velocity ($m\ s^{-1}$)
G_S	static gain of the low pass filter
T	nondimensional growth velocity oscillation period
T_c	nondimensional cut-off period
t	nondimensional time
S	elongation factor
u, v	nondimensional convective velocity components
X, Z	space coordinates (m)
x, z	nondimensional space coordinates
v_i	nondimensional interface velocity
Gr	Grashof number
Sc	Schmidt number
Pe	Peclet number
Pr	Prandtl number

Greek letters

β	expansion coefficient (K^{-1})
δ	solute boundary layer thickness (m)
Δ	convecto diffusive parameter ($0 \leqslant \Delta \leqslant 1$)
ν	kinematic velocity of the melt ($m^2\ s^{-1}$)
ρ	mass density ($kg\ m^{-3}$)
α	amplitude of growth velocity oscillation
Θ	dimensional temperature
Θ_I	dimensional interface temperature
θ	nondimensional temperature
ω	pulsation of the perturbation (s^{-1})
Ω	nondimensional pulsation of growth velocity fluctuation, $\Omega = \omega\delta^2/D$
Ω_c	nondimensional cut-off pulsation
∇	Nabla operator

assumption, obviously questionable from a physical standpoint, was dropped, and a solution obtained in the sounder frame of the boundary layer model [9].

Numerical simulations are another fruitful way to approach the problem of transient solute incorporation. Interesting results were thus obtained by Wilson [10], or more recently by Jung and Müller [11], respectively, in Czochralski and vertical Bridgman configurations. In both cases, the agreement with the predictions of the analytical [8,9] or semi-analytical [12] models was fair; however, the amount of computer resources necessary to solve the unsteady transport equations is still considerable. Only a few test cases were thus simulated, so that no general conclusion regarding the accuracy of the models can be drawn.

The purpose of the present paper is to study in detail the effect of a fluctuation of the growth velocity on the crystal composition. To do so, we carry out numerical simulations of the transport phenomena in a horizontal Bridgman configuration. The induced variations of both axial and radial solute segregation are characterized. Since our objective is to conduct a full parametric study, the imposed fluctuations of the growth velocity cover a large amplitude and frequency range. In order to gain some insight into the physics of the problem, the obtained numerical results are compared with the predictions of a simplified analytical model based on the solutal boundary layer concept.

Indeed, previous numerical studies [13] clearly showed that the convecto-diffusive parameter Δ, that measures the relative contributions of diffusion and convection to mass transport [14], accounted adequately for macrosegregation phenomena. Let us recall that Δ is defined as the ratio of the dimensional solutal boundary layer thickness δ to its reference value in diffusion-controlled conditions D/V_I, yielding $\Delta = \delta V_I/D$, and that Δ can be estimated from experimental or numerical axial segregation profiles using the effective partition ratio concept [7,14]. In any case, it was tempting to see whether an analytical approach, based on this parameter Δ, could capture the physics of transient solute segregation.

We shall first recall in Section 2 the main features of a simplified analytical model accounting for the effect of unsteady growth velocity on composition.

Then, in Section 3, the physical model and the numerical procedure are briefly presented. Section 4 is dedicated to the analysis of the simulation results. A discussion of the accuracy of the analytical model, and of its ability to capture the physics of solute transport phenomena both in quasi-steady and transient problems, is also carried out.

2. Outline of the analytical solution

Our purpose in this section is to briefly recall the main features of an analytical model that allows to derive the composition response to a given growth velocity perturbation, since it will be thoroughly used in the following for comparison with the numerical results. For more details on the starting assumptions and the procedure, the interested reader is referred to the original publication [9]. To start with, let us consider the time-dependent mass conservation equation, written in a reference frame moving with the interface:

$$\partial C/\partial t + (\boldsymbol{V}\cdot\nabla)C = D\nabla^2 C + (\boldsymbol{V}_I\cdot\nabla)C. \quad (1)$$

In the above equation, C, D, $\boldsymbol{V}$ and $\boldsymbol{V}_I$, respectively, stand for solute concentration and diffusion coefficient, convection velocity and growth rate. A first assumption is to drop the radial composition derivatives, that is to suppose that the concentration variations take place principally along the normal to the interface, X in the notations of the present paper. However, the key idea is to account for convective effects using an effective transport velocity, yielding:

$$\partial C/\partial t = D\partial^2 C/\partial X^2 + V_{\text{eff}}\partial C/\partial X, \quad (2)$$

where V_{eff} can be related to the solutal boundary layer thickness δ of the associated steady-state problem through $V_{\text{eff}} = D/\delta$ [9,14]. Then, in line with the approach originally proposed by Hurle et al. [6], a solution to Eq. (2) is obtained through a Fourier series expansion up to the order one of the main variables of the problem. For instance, the form of the composition field is given as

$$C(X,t) = C^0(X) + C^1(X)\exp(\mathrm{j}\omega t). \quad (3)$$

The interface velocity fluctuation V_I^1 is assumed small enough to neglect the second-order term $V_I^1 C^1$ in Eq. (2). Even with these assumptions, the algebra involved is fairly tedious, and the interested reader is referred to the original publication [9] for details on the derivation. However, for our present purposes, a composite solution can be built based on the asymptotic high-frequency and low-frequency regimes [9,15]. Sufficiently far away from the diffusive transport limit, the relation between normalized growth rate and interface composition fluctuations can be expressed as

$$C_I^1/C_I^0 = [G_S/(1 + \mathrm{j}\Omega/\Omega_C)^{1/2}]V_I^1/V_I^0, \quad (4)$$

where the non-dimensional pulsation Ω is defined as $\Omega = \omega\delta^2/D$. The variables G_S and Ω_C, respectively, stand for the static gain and the cutoff pulsation of this order $\frac{1}{2}$ linear filter and j the complex number such that $\mathrm{j}^2 = -1$. Numerically, G_S and Ω_C are given as

$$G_S = (1-k)\Delta(1-\Delta)/[1-(1-k)\Delta], \quad (5)$$

$$\Omega_C = [(1-(1-k)\Delta)/(1-\Delta)]^2. \quad (6)$$

As noted in Ref. [6], the occurrence of imaginary terms is related to a phase shift between the growth velocity and interface composition fluctuations. It should be noted that the Δ featured in expressions (5) and (6) should be deduced from the analysis of axial macrosegregation profiles based on the mean growth velocity.

3. Physical model and numerical procedure

We consider the directional solidification of a diluted binary alloy, which will be supposed to be Newtonian, incompressible and to obey Boussinesq approximation. The studied configuration is schematically represented in Fig. 1 and corresponds to

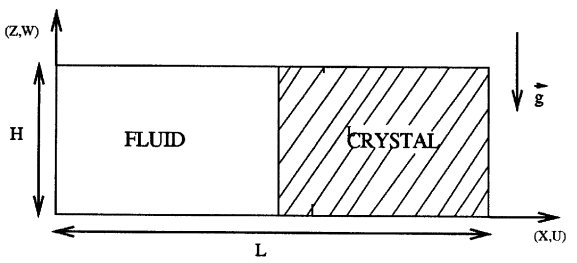

Fig. 1. Studied configuration.

a cavity of aspect ratio: $A = L/H$ where L is the length of the cavity and H its height. The crystal–fluid interface will be supposed to be planar. We solve numerically the Navier–Stokes equations coupled to those of energy and species conservation. We use the vorticity–stream function formulation which is appropriate for the case of two-dimensional flows.

Let the reference variables be: H for distance, v/H for velocity, H^2/v for time, $\nabla\Theta * H$ for temperature ($\nabla\Theta$ is the thermal gradient) and C_0 (initial solute concentration in the melt) for concentration. The domain containing the melt varies during the solidification process. It is transformed in a fixed domain using the following transformation: $x = X/S(t)$ and $z = Z$, where $S(t)$ is the dimensionless length of the liquid area. According to these tranformations, the dimensionless governing equations in the liquid phase are then written as

$$\frac{\partial\zeta}{\partial t} + (u - xv_i)\frac{1}{S}\frac{\partial\zeta}{\partial x} + w\frac{\partial\zeta}{\partial z} = \frac{1}{S^2}\frac{\partial^2\zeta}{\partial x^2} + \frac{\partial^2\zeta}{\partial z^2} - \mathrm{Gr}\frac{1}{S}\frac{\partial\theta}{\partial x},$$

$$\frac{1}{S^2}\frac{\partial^2\psi}{\partial x^2} + \frac{\partial^2\psi}{\partial z^2} = -\zeta,$$

$$\frac{\partial\theta}{\partial t} + (u - xv_i)\frac{1}{S}\frac{\partial\theta}{\partial x} + w\frac{\partial\theta}{\partial z} = \frac{1}{\mathrm{Pr}}\left[\frac{1}{S^2}\frac{\partial^2\theta}{\partial x^2} + \frac{\partial^2\theta}{\partial z^2}\right],$$

$$\frac{\partial c}{\partial t} + (u - xv_i)\frac{1}{S}\frac{\partial c}{\partial x} + w\frac{\partial c}{\partial z} = \frac{1}{\mathrm{Sc}}\left[\frac{1}{S^2}\frac{\partial^2 c}{\partial x^2} + \frac{\partial^2 c}{\partial z^2}\right],$$

where ζ, ψ, θ and c are the dimensionless variables for, respectively, the vorticity, the stream function, the temperature ($\theta = (\Theta - \Theta_I)/(\nabla\Theta * H)$, where Θ_I is the temperature of the interface) and the concentration. u and w are the convective velocity components defined as: $u = \partial\psi/\partial z$ and $w = -\partial\psi/\partial x$; v_i is the dimensionless solid–liquid interface velocity, so that $v_i = V_I * H/v$. v_i will be assumed to vary periodically as

$$v_i(t) = v_0(1 + \alpha\sin(2\pi t/T)),$$

where v_0 is the average velocity value which will be taken as $v_0 = 0.2$, α is the amplitude of interface velocity fluctuations and T the period of these fluctuations. The governing equations feature the nondimensional numbers of Grashof, $\mathrm{Gr} = g\beta H^4\nabla\Theta/v^2$, Prandtl, $\mathrm{Pr} = v/\kappa$ and Schmidt, $\mathrm{Sc} = v/D$.

To these basic equations, need to be added the equations related to the boundary conditions. At any instant, the amount of solute being incorporated in the solid is taken to be proportional to the amount of solute in the melt at the interface, so that

$$c_s = kc_l.$$

k is the equilibrium partition ratio, the indices s and l, respectively, relate to the solid and liquid phases. The balance equation of mass conservation at the solid–liquid interface is written as

$$\frac{\partial c}{\partial x} = \mathrm{Pe}(1 - k)c,$$

where Pe is the Péclet number: $\mathrm{Pe} = HV_I/D$. The other boundaries of the melt are supposed to be solid and impermeable and various thermal conditions can be applied along them. In this study, we will impose a linear temperature profile, variable between two extreme temperatures on the lateral side walls. The mesh used is generated by Thompson technique [16]. The nodes are squeezed near the walls of the cavity and especially in the vicinity of the solid–liquid interface because of high composition gradients there. The problem is solved by using a Hermitian finite difference method with an alternative implicit direction scheme in a grid of 25×101 points on (z, x) directions [17]. In our numerical computations, a cavity of aspect ratio $A = 4$ is used and the solidification was conducted over the first half of the cavity. We shall focus on two quantities: the amplitude of the normalized segregation oscillations and their phase shift with respect to the imposed interface velocity.

4. Results

4.1. General characteristics

4.1.1. Response of the concentration to the fluctuating interface velocity

We present in Fig. 2 a typical case of unsteady growth velocity with $\alpha = 0.85$ and $T = 0.5$ and the

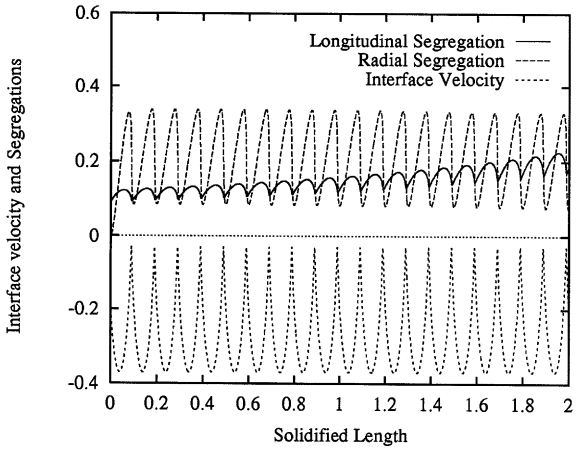

Fig. 2. Segregation responses to the fluctuating velocity.

segregation responses. The fluctuating interface velocity and the longitudinal and radial segregations are given according to the solidified length. Let us recall that the longitudinal (or axial) segregation C_l is defined as the average value of the dopant concentration along the growth interface, while the radial segregation C_r is defined as follows:

$$C_r = \frac{C_{lmax}(z) - C_{lmin}(z)}{C_l}.$$

We note in Fig. 2 that the variation of the velocity which is taken sinusoidal according to time, loses its sinusoidal character according to space while remaining periodic. The variation observed will be more distant from a sinusoid as the amplitude is larger. The value $\alpha = 1$ constitutes a limiting amplitude that we do not want to exceed, because beyond this value the system presents intervals of time where the solid–liquid interface moves back, and our model is not adapted to taking into account such a remelting of the crystal.

We also see that in response to the oscillatory growth velocity, the longitudinal and radial segregations vary periodically with the same period than the interface velocity variations. We remark that the amplitude of the radial segregation quickly tends to be constant, when the longitudinal segregation increases during the solidification process. This figure also indicates that the concentration cycle lags behind the growth velocity cycle.

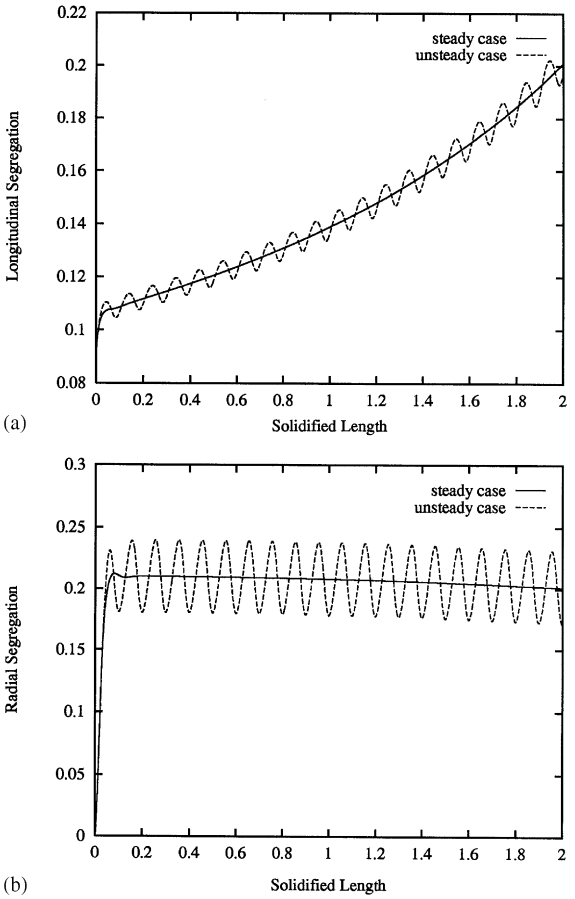

Fig. 3. Segregation responses. (a) Longitudinal segregations for steady and unsteady cases. (b) Radial segregations for steady and unsteady cases.

4.1.2. Comparison with the case $v_i = v_0$

We plot in Fig. 3a and Fig. 3b, respectively, the longitudinal and radial segregation profiles in the crystal when the solid–liquid interface velocity varies with an amplitude $\alpha = 0.2$ and $T = 0.5$ along with those corresponding to a constant growth of the interface $v_i = v_0$. We note that the segregations for the unsteady case take place on both sides of the corresponding segregations relative to the steady case.

Let us look now at the longitudinal and radial concentration behaviors in more detail, as functions of the amplitude and the frequency of the interface velocity variations.

4.2. Longitudinal segregation

4.2.1. Effect of the perturbation amplitude

We studied the influence of the amplitude of interface velocity variations on the solute distribution in the crystal for a fixed period $T = 0.5$. In Fig. 4 we present the longitudinal segregation for three values of α, $\alpha = 0.2$, 0.5 and 0.85. We note that the amplitude of segregation signals increases when the amplitude of growth velocity increases. For a better exploitation of our results and also for a more direct comparative study with the analytical and experimental results of Garandet [9] and Corre [15], it seems interesting to normalize the oscillatory signals of segregation by the values obtained at the steady growth rate $v_i(t) = v_0$. In the same manner as Garandet [9], we define a normalized longitudinal segregation C_n as

$$C_n = \frac{C_{lv} - C_{lc}}{C_{lc}},$$

where C_{lv} is the longitudinal segregation at the variable growth rate and C_{lc} the longitudinal segregation at the constant growth rate. Normalization appears particularly suitable since the oscillatory signals of longitudinal segregation have now a constant amplitude in the course of time and thus can be characterized much better (see Fig. 5). Let us try to bring out now the evolution of the value of this amplitude with α. We also pay attention to the phase shift between the oscillations signals of interface velocity and the response of the segregation in the crystal. We illustrate in Fig. 6a, the variation of the amplitude of normalized longitudinal segregation over the considered range of α values. It is remarkable that, even close to remelting situations at $\alpha = 0.85$, the system behaves linearly. Such a behavior supports the use of a linearized analytical model based on small amplitude fluctuations. Fig. 6b indicates that, at this oscillation period $T = 0.5$, the amount by which the longitudinal segregation lags behind the interface velocity is constant and equal to $\sim \pi/6$.

4.2.2. Effect of the perturbation period

We studied the effect of the period of oscillations for a fixed amplitude of the velocity disturbance $\alpha = 0.2$. The evolution of the normalized longitudinal segregation amplitude $|C_n|$ according to the period T is represented in Fig. 7a where we plot the profile of the analytical model along with the numerical results in a logarithmic scale. We confirm the existence of an asymptotic mode for the small periods (given by Garandet [9]) and an asymptotic limit for the large periods. The figure indicates that the analytical curve approximates well the numerical points until $T = 0.6$, value beyond which the amplitude of the segregation signal can be taken as constant. An interpretation of this behavior would be to say that an oscillatory excitation of the system at a high frequency does not leave it enough time to

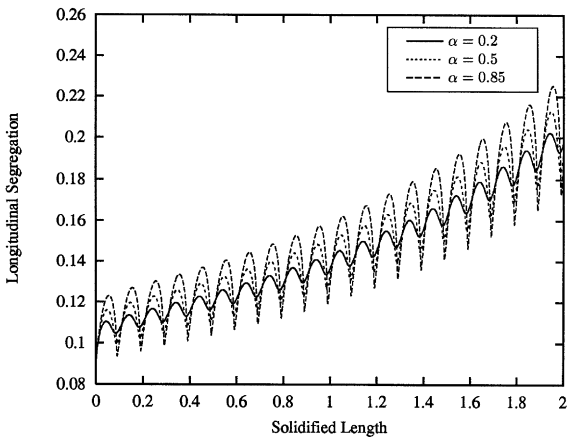

Fig. 4. Longitudinal segregation for different α ($T = 0.5$).

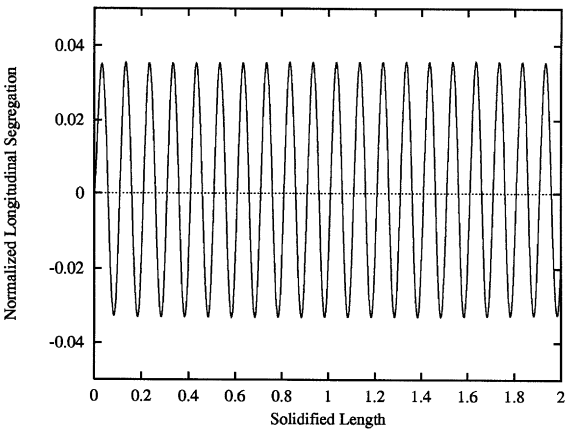

Fig. 5. Normalized longitudinal segregation ($\alpha = 0.2$, $T = 0.5$).

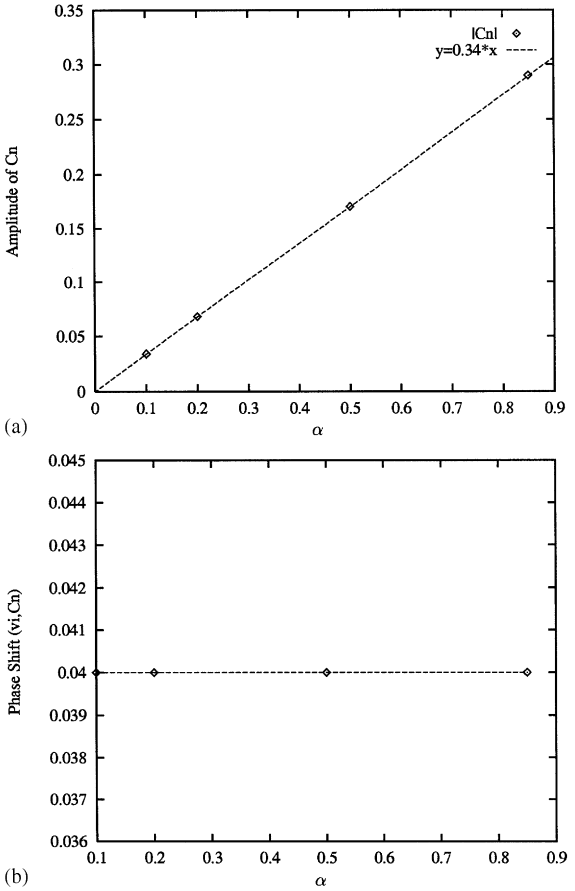

Fig. 6. Amplitude and phase shift of $|C_n|$ ($T = 0.5$). (a) Variation of the amplitude $|C_n|$ with α. (b) Phase shift $\phi(v_i, C_n)/4\pi$ as a function of α.

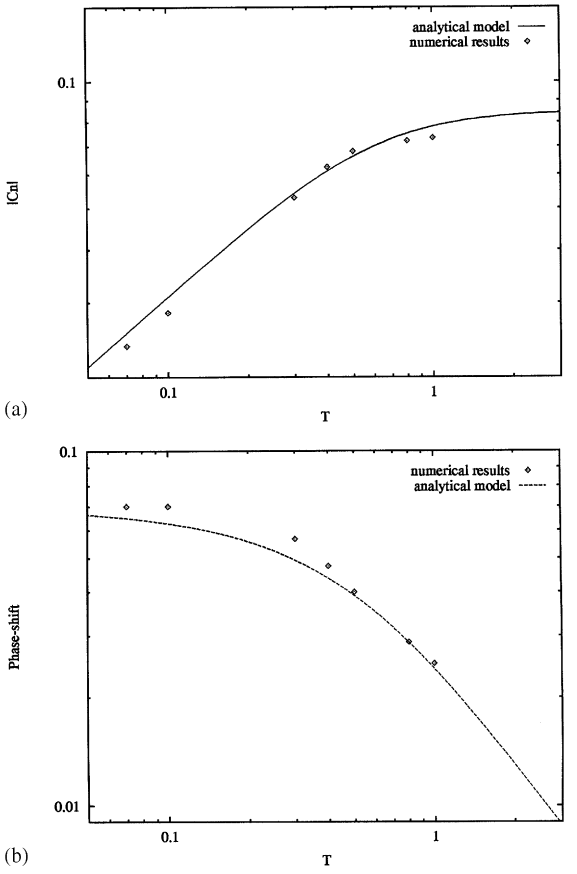

Fig. 7. Amplitude and phase shift of $|C_n|$ ($\alpha = 0.2$). (a) Variation of the amplitude $|C_n|$ with T. (b) Phase shift $\phi(v_i, C_n)/4\pi$ as a function of T.

adapt to the variations which it undergoes; conversely, the lower the frequency, the more this adaptation is possible.

We present in Fig. 7b the variation of the phase shift between the periodic interface velocity and longitudinal segregation signals. The numerical results are plotted along with the analytical model profile. We see that this phase shift seems rather constant, and equal to $\sim \pi/4$, for the small periods ($T \leqslant 0.1$), and that it then decreases strongly beyond this value of T. This result also confirms the theoretical value of the phase shift predicted by Garandet [9] for the small periods (see Section 5).

4.3. Radial segregation

As for the longitudinal segregation, we choose to normalize the radial segregation before trying to have some insight into the correlation between interface velocity variation and radial segregation in the crystal from our numerical computations. We define the normalized radial segregation $C_{n'}$ as

$$C_{n'} = C_{rv} - C_{rc},$$

where C_{rv} is the radial segregation at variable growth rate and C_{rc} at constant growth rate. Indeed, this choice enables us to obtain a segregation oscillating with constant amplitude (Fig. 8).

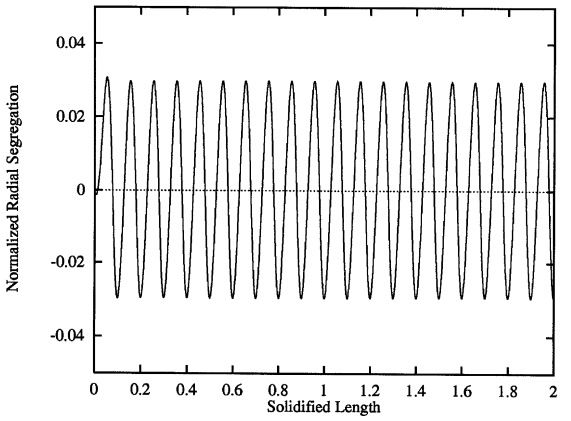

Fig. 8. Normalized radial segregation ($\alpha = 0.2$, $T = 0.5$).

4.3.1. Effect of the perturbation amplitude

For the radial segregation, we illustrate in Fig. 9a the linear variation of the amplitude of this normalized segregation according to α, for a perturbation period $T = 0.5$.

In Fig. 9b, we then present the phase shift between the signals of interface velocity and response in radial segregation.

We thus observe that this phase shift is constant and equal to $\pi/2$, at $T = 0.5$, for all values of α.

4.3.2. Effect of the perturbation period

The variation of the amplitude of the normalized radial segregation in the crystal at $\alpha = 0.2$, according to the variation of the growth velocity period is given in Fig. 10a, in a logarithmic scale. The segregation profile is plotted along with the curve of the fit with order 2.35 filter. This figure demonstrates an asymptotic behavior of $|C_{n'}|$ for the small periods T and an asymptotic limit reached at $T \sim 0.55$. As for the phase shift between the velocity and the segregation signals, we obtain a constant value equal to $\sim 4\pi/3$ for the small periods ($T < 0.1$), whereas beyond this value the phase shift decreases in a significant way when the period T increases (see Fig. 10b).

4.4. Illustration of the striations in the crystal

Fig. 11 shows the segregation in the solidified alloy for various cases of oscillation of v_i. We note

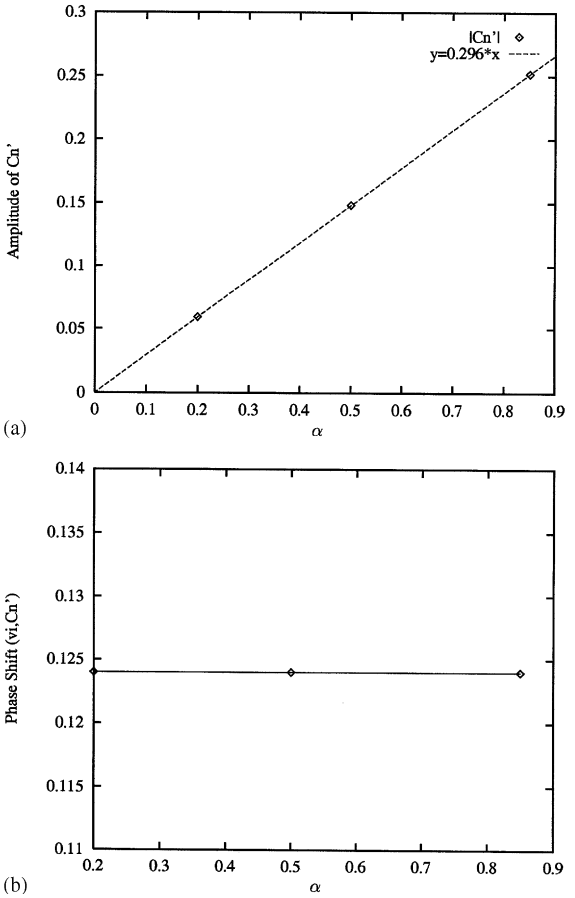

Fig. 9. Amplitude and phase shift of $|C_{n'}|$ ($T = 0.5$). (a) Variation of the amplitude $|C_{n'}|$ with α. (b) Phase shift $\phi(v_i, C_{n'})/4\pi$ as a function of α.

that the structure of the solid sample depends directly on the oscillation and in particular notice, as explained previously, that in the case of an oscillation with a small period, the system has not enough time to adapt to the interface velocity variations, which results in a structure very close to that corresponding to a solidification at constant growth rate.

5. Discussion

Using the identity $\delta = \Delta(D/V_I)$, the relation between the pulsation Ω of the analytical model and

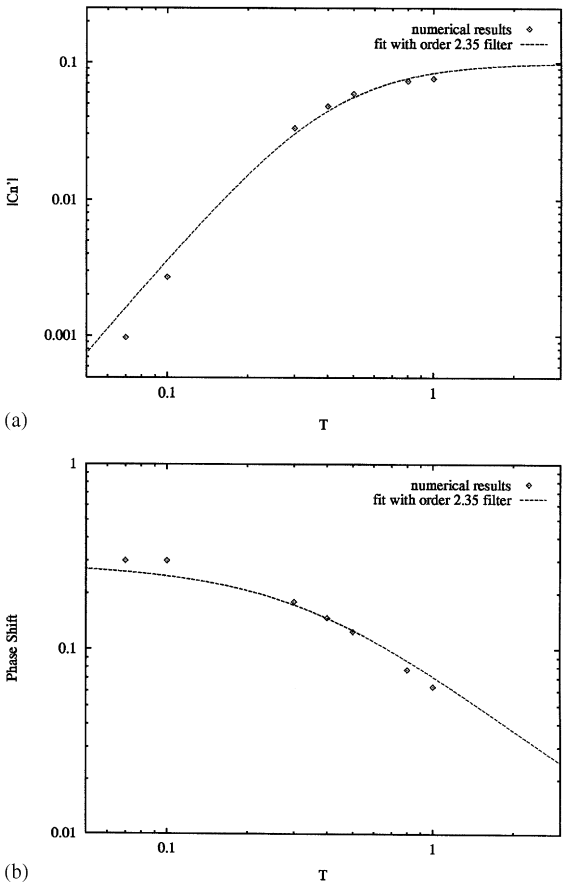

Fig. 10. Amplitude and phase shift of $|C_{n'}|$ ($\alpha = 0.2$). (a) Variation of the amplitude $|C_{n'}|$ with T. (b) Phase shift $\phi(v_i, C_{n'})/4\pi$ as a function of T.

the period T of the numerical simulations can be written as

$$\Omega = \omega\delta^2/D = 2\pi \,\mathrm{Sc}\,\mathrm{Pe}^{-2}\Delta^2 T^{-1}.$$

The nondimensional numbers of Schmidt and Péclet are fixed in the present study, $\mathrm{Sc} = 10$ and $\mathrm{Pe} = 2$. The value of the convecto-diffusive parameter, deduced from the numerical results on macrosegregation [13], is also constant in the frame of this work, $\Delta = 0.2$. Using this value in Eqs. (5) and (6), we get $G_S = 0.18$ and $\Omega_C = 1.04$. The cut-off nondimensional period T_C is thus $T_C = 0.6$. The predictions of the analytical model (Eq. (4)) are represented in Fig. 7a and Fig. 7b along with the numerical data. Keeping in mind that Δ is not an adjustable parameter, the agreement can be considered excellent, both in terms of amplitude and phase shift.

As for comparison with experimental data, a series of key papers were published by the MIT team [18–20] in the 1970s. Direct and simultaneous measurements of dopant concentration (via spreading resistance) and interface velocity (via Peltier pulse marking) were carried out on Czochralski-grown Si- and Ge-based alloys. An analysis of the experimental results showed that the predictions of the analytical model were fair, with a maximum discrepancy of the order of 50%. Considering the very good agreement between numerical and analytical data apparent in the present paper, it is unlikely that the numerical simulations could account significantly better for the experimental results. To bridge the remaining discrepancy, kinetic mechanisms could be invoked [21,22], but the reader should keep in mind that in such a complex problem, a 50% agreement can be considered satisfactory. Our opinion is that, in contradiction with the data presented by Carruthers [21], macroscopic transport phenomena play a key role in the physics of transient solute transport incorporation.

Regarding radial segregation, no analytical model is available for comparison with the numerical results. However, one can notice that the phase shift between the growth rate and composition fluctuations is much higher than for axial segregation. This can be qualitatively understood by the fact that the spatial range of the concentration gradient is larger in the radial case (H versus δ). The time needed for a composition information to travel along the interface is thus necessarily higher, but no explanation is available to this day to account for the filter behavior of radial segregation more specifically. Too much emphasis should not be laid to the 2.35 exponent that results from a best-fit procedure and not from a physical model.

6. Concluding remarks

Our purpose in this work was to analyze in detail the effect of a growth rate fluctuation on solute incorporation. Numerical simulations of the heat, momentum and mass transport phenomena in

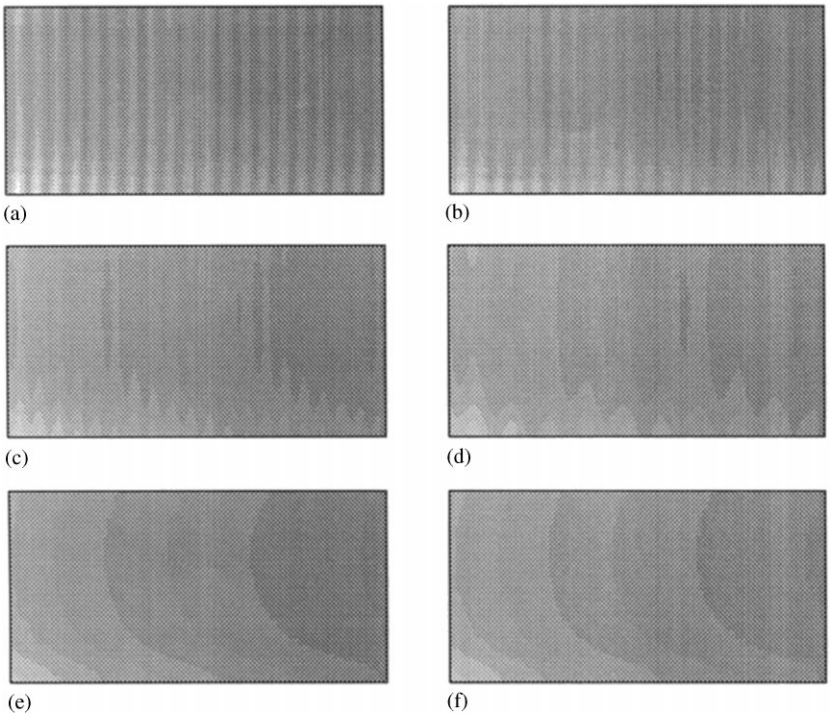

Fig. 11. Solute distribution in solidified alloy for different values of α and T. (a) $\alpha = 0.85$, $T = 0.5$. (b) $\alpha = 0.5$, $T = 0.5$. (c) $\alpha = 0.2$, $T = 0.5$. (d) $\alpha = 0.2$, $T = 1.0$. (e) $\alpha = 0.2$, $T = 0.1$. (f) nonoscillatory case.

a horizontal Bridgman configuration were thus carried out. The imposed variations of the solidification velocity covered a large amplitude and frequency range. It was seen that the induced axial and radial segregation can be quite large. The agreement of the numerical results with the predictions of a simplified analytical model based on the solutal boundary layer concept was very good. Remembering its past sucesses [14], the ability of the boundary layer model to efficiently capture the physics of the solute transport phenomena in both steady state and transient problems is thus remarkable.

To finish with, a practical point is worth stating. In many actual growth configurations, convection controls solute transport. The parameter Δ is thus often fairly small, meaning that the cutoff frequency Ω_C will be of the order of magnitude unity (see Eq. (6)). In dimensional terms, the condition is thus $\omega_C \cong D/\delta^2$. Taking typical values $D = 10^{-8}\,m^2\,s^{-1}$ and $\delta = 10^{-4}\,m$, we get $\omega_C \cong 1\,s^{-1}$. Higher frequency perturbations, e.g. associated with machinery operation, should then be significantly damped. On the other hand, special care should be devoted to the optimization of pulling velocity or thermal regulation, that act at the low-frequency end of the spectrum.

Acknowledgements

The present work has been conducted within the frame of the "Action de Recherche Amont" between the ECL and the CEREM. The contribution of J.P. Garandet is part of the Gramme agreement between the CNES and the CEA.

References

[1] J.R. Carruthers, A.F. Witt, in: R. Ueda, J.B. Mullin (Eds.), Crystal Growth and Characterization, North-Holland, Amsterdam, 1975.

[2] A.F. Witt, M. Lichtensteiger, H.C. Gatos, J. Electrochem. Soc. 120 (1973) 1119.
[3] J.I.D. Alexander, J. Ouazzani, F. Rosenberger, J. Crystal Growth 97 (1989) 285.
[4] T. Nishinaga, T. Kazuno, T. Tanbo, J. Koide, K. Pak, T. Nakamura, Y. Yasuda, J. Crystal Growth 65 (1983) 607.
[5] A.N. Danilewsky, K.W. Benz, J. Crystal Growth 97 (1989) 571.
[6] D.T.J. Hurle, E. Jakeman, E.R. Pike, J. Crystal Growth 3 (4) (1968) 633.
[7] J.A. Burton, R.C. Prim, W.P. Slichter, J. Chem. Phys. 21 (1953) 1987.
[8] D. Thevenard, A. Rouzaud, J. Comera, J.J. Favier, J. Crystal Growth 108 (1991) 572.
[9] J.P. Garandet, J. Crystal Growth 131 (1993) 431.
[10] L.O. Wilson, J. Crystal Growth 48 (1980) 435 and 451.
[11] T. Jung, G. Müller, J. Crystal Growth 171 (1997) 373.
[12] J.J. Favier, L.O. Wilson, J. Crystal Growth 58 (1982) 103.
[13] S. Kaddeche, H. Ben Hadid, D. Henry, J. Crystal Growth 135 (1994) 341.
[14] J.P. Garandet, J.J. Favier, D. Camel, in: D.T.J. Hurle (Ed.), Handbook of Crystal Growth, Vol. 2, North-Holland, Amsterdam, 1994.
[15] S. Corre, Ph.D. Thesis, INP-Grenoble, 1997.
[16] J.F. Thompson, Z. Vawarsi, C.W. Mastin, Numerical Grid Generation, Elsevier, Amsterdam, 1985.
[17] R. Hirsh, J. Comput. Phys. 19 (1975) 90.
[18] A.F. Witt, M. Lichtensteiger, H.C. Gatos, J. Electrochem. Soc. 120 (1973) 1119.
[19] A. Murgai, H.C. Gatos, A.F. Witt, J. Electrochem. Soc. 123 (1976) 224.
[20] A. Murgai, H.C. Gatos, W.A. Westdorp, J. Electrochem. Soc. 126 (1979) 2240.
[21] J.R. Carruthers, Can. Metall. Quart. 5 (1966) 55.
[22] H.U. Walter, J. Electrochem. Soc. 123 (1976) 1098.